

# We are IntechOpen, the world's leading publisher of Open Access books Built by scientists, for scientists

6,900

Open access books available

186,000

International authors and editors

200M

Downloads

Our authors are among the

154

Countries delivered to

TOP 1%

most cited scientists

12.2%

Contributors from top 500 universities



WEB OF SCIENCE™

Selection of our books indexed in the Book Citation Index  
in Web of Science™ Core Collection (BKCI)

Interested in publishing with us?  
Contact [book.department@intechopen.com](mailto:book.department@intechopen.com)

Numbers displayed above are based on latest data collected.  
For more information visit [www.intechopen.com](http://www.intechopen.com)



---

# Planar Microstrip-To-Waveguide Transition in Millimeter-Wave Band

---

Kazuyuki Seo

Additional information is available at the end of the chapter

<http://dx.doi.org/10.5772/54662>

---

## 1. Introduction

Many kind of millimeter-wave automotive radars have been developed [1], [2]. The microstrip antenna becomes a good candidate when radar sensors are widely used in vehicle due to its advantages of low cost and low profile. Generally microstrip antennas are placed on the surface of a radar sensor and are connected to millimeter-wave circuits inside of the sensor via waveguides. Therefore, transitions from waveguide to microstrip line are required, as shown in Figure 1.

Rectangular waveguides were one of the earliest types of transmission lines used to transport microwave signals and are still used today for many applications. Because of the recent trend toward miniaturization and integration, a lot of microwave circuitry is currently fabricated using planar transmission lines, such as microstrip or strip line, rather than waveguide. There is, however, still a need for waveguides in many applications such as millimeter wave systems, and in some precision test applications.

Various types of millimeter-wave transitions from waveguide to microstrip line have been proposed. The ridge waveguide type [3], quasi-Yagi type [4], and planar waveguide type [5] have been studied as longitudinal connection of waveguide with microstrip line. With regard to vertical transitions, a conventional type of probe feeding has a wideband characteristic [6], [7], but it needs a metal short block with a quarter-wavelength on the substrate. The replacement of the metal short block is a patch element in the waveguide to achieve sufficient coupling between waveguide and microstrip line. The slot coupling type [8] achieves coupling between the microstrip line and the patch element in the waveguide by means of a slot, it is composed of two dielectric substrates without a metal short block. The proximity coupling type [9] has been developed more recently. It can be composed of a single dielectric substrate attached to the waveguide. A rectangular patch element on the lower plane of the dielectric substrate

couples with a microstrip line on the upper plane of the dielectric substrate. It is suitable for mass production. The proximity coupling type has been further developed for wideband [10].

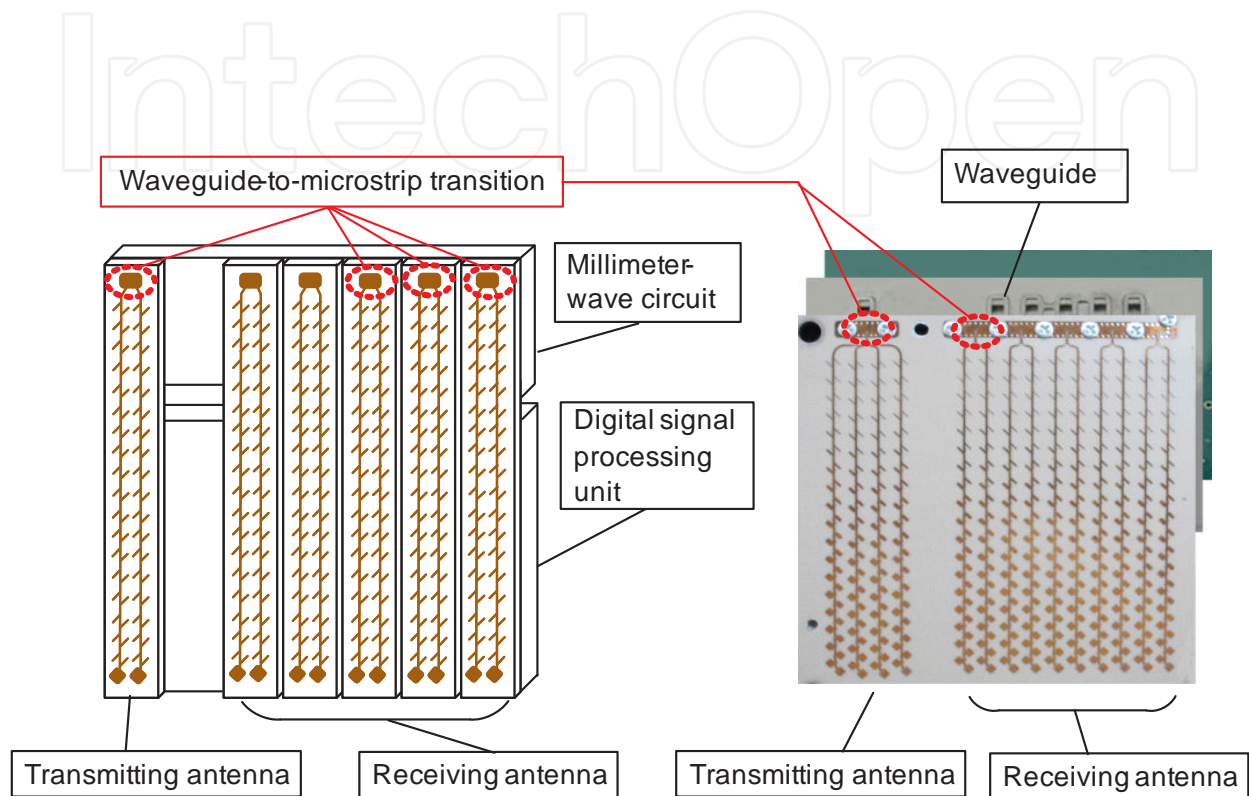


**Figure 1.** Construction of millimeter-wave automotive radar sensor and photograph for example

## 2. Probe transition with back-short

The transitions with short-circuited waveguide of  $1/4$  guided wavelength on the substrate are very popular [6], [7] because their principle of mode transformation is almost the same with that of ordinary transitions of a waveguide and a coaxial cable [11]. The probe transition connects a microstrip line and a waveguide as shown in Figure 2. A probe at one end of the microstrip line is inserted into the perpendicular waveguide whose one end is short-circuited by the back-short waveguide.

The configuration is shown in Figure 3. A dielectric substrate with conductor patterns on its both sides is placed on an open-ended waveguide (WR-12 standard waveguide). An aperture of the substrate is covered with an upper waveguide. A short circuit of the upper

waveguide is essentially  $\lambda_g/4$  ( $\lambda_g$ : guided wavelength of the waveguide) above the substrate. Consequently, the electric current on the probe couples to the magnetic field of  $TE_{10}$  dominant mode of the waveguide as shown in Figure 4. Via holes are surrounding the waveguide in the structure in order to reduce the leakage of parallel plate mode transmitting into the substrate. Impedance matching could be achieved by controlling the length  $\rho$  of the probe and the length  $S_s$  of the upper waveguide. Each parameters in Figure 3 are shown in Table 1 for example.

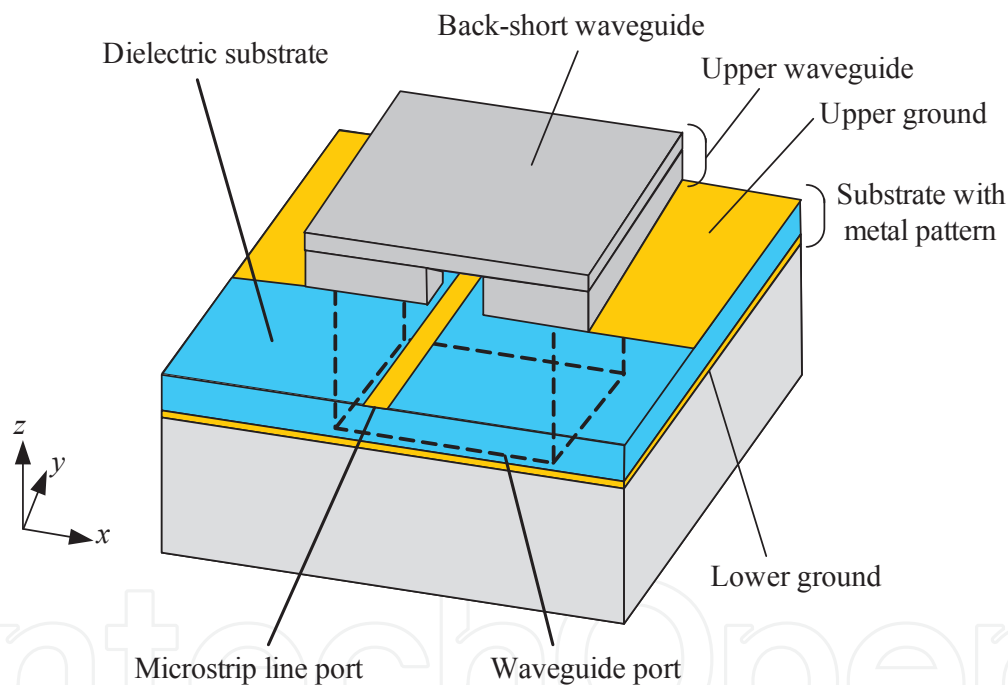


**Figure 2.** Probe transition with back-short

In order to reduce the leakage from the waveguide window at the insertion of the microstrip line, the width of the window should be narrow than the width of the cut off condition and is 0.9 mm in this case. S-parameters of the reflection  $S_{11}$  and the transmission  $S_{21}$  are calculated by using an electromagnetic simulator based on the finite element method (Ansys HFSS) as shown in Figure 5. From the simulated results, this transition has wide frequency bandwidth.

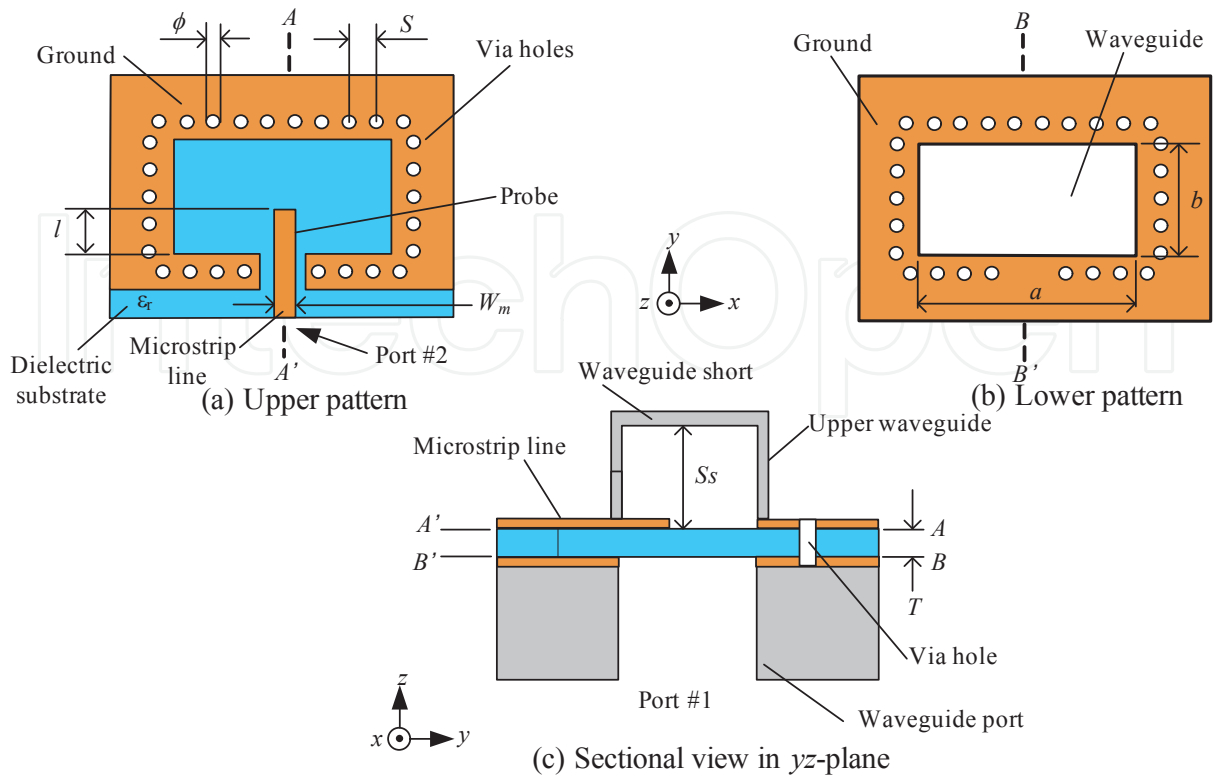


Figure 3. Detailed configuration of the probe transition with back-short

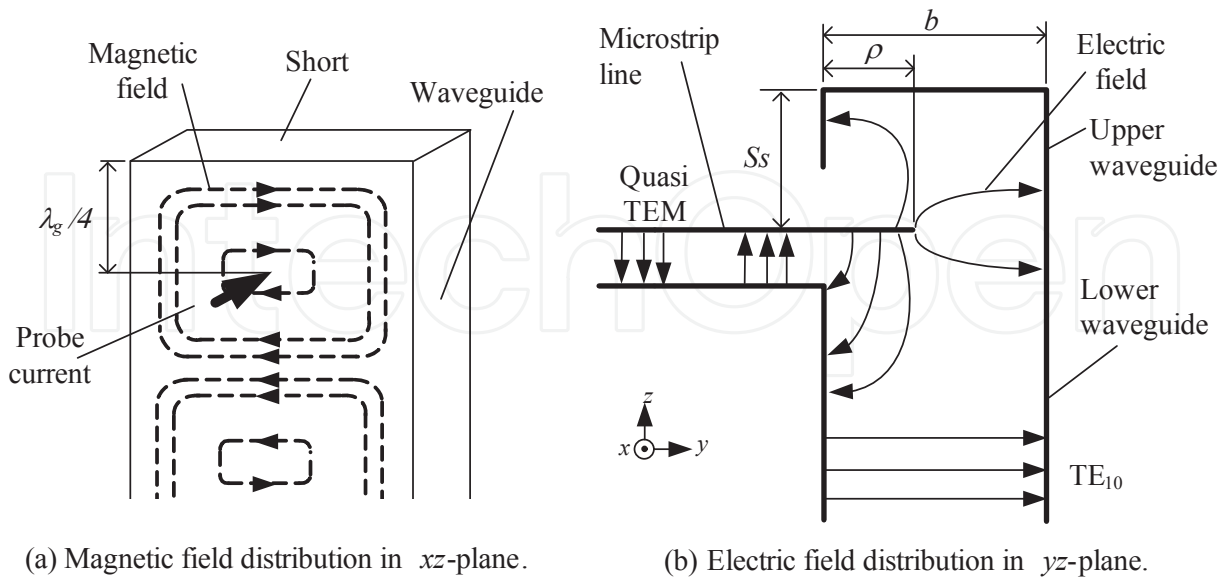
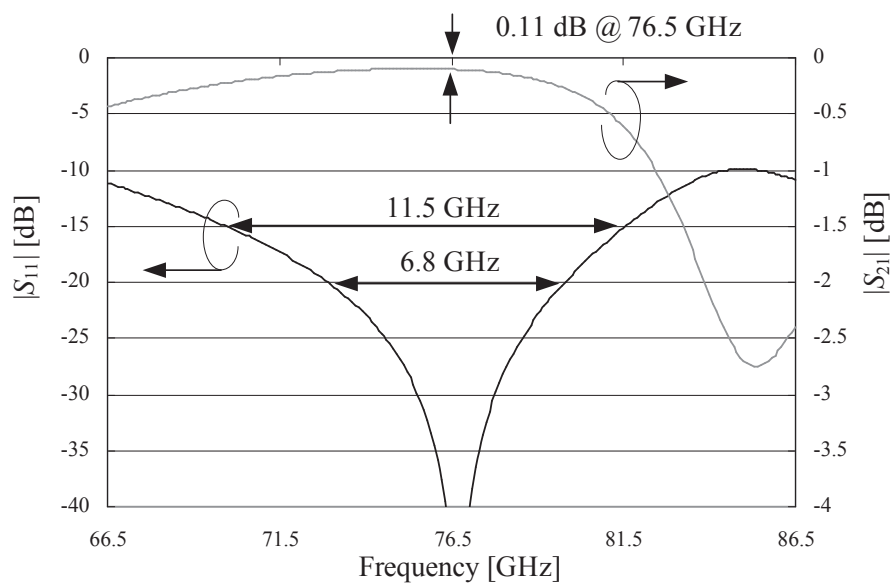


Figure 4. Magnetic and electric field lines

Description	Name	Value (mm)	Description	Name	Value (mm)
Broad wall length of waveguide	$a$	3.1	Narrow wall length of waveguide	$b$	1.55
Width of microstrip line	$W_m$	0.3	Length of inserted probe	$\rho$	0.675
Length of back short waveguide	$S_s$	0.61	Relative permittivity	$\epsilon_r$	2.2
Thickness of substrate	$T$	0.127	Diameter of via hole	$\phi$	0.2
Space between via holes	$S$	0.5			

**Table 1.** Parameters of probe transition with back-short



**Figure 5.** Reflection characteristic  $|S_{11}|$  and insertion loss  $|S_{21}|$  of probe transition with back-short

### 3. Planar proximity coupling transition

Planar proximity coupling transitions shown in Figure 6 and Figure 7 have been proposed [9]. This transition can be composed of only a single dielectric substrate attached to the waveguide end and suitable for mass production. The conductor pattern with a notch (it is named a waveguide short pattern because of its function) and the microstrip line are located on the upper plane of the dielectric substrate. A rectangular patch element and a surrounding ground are patterned on the lower plane of the dielectric substrate. Via holes are surrounding the aperture of the waveguide on the lower plane of the dielectric substrate to connect the surrounding ground and the waveguide short electrically.

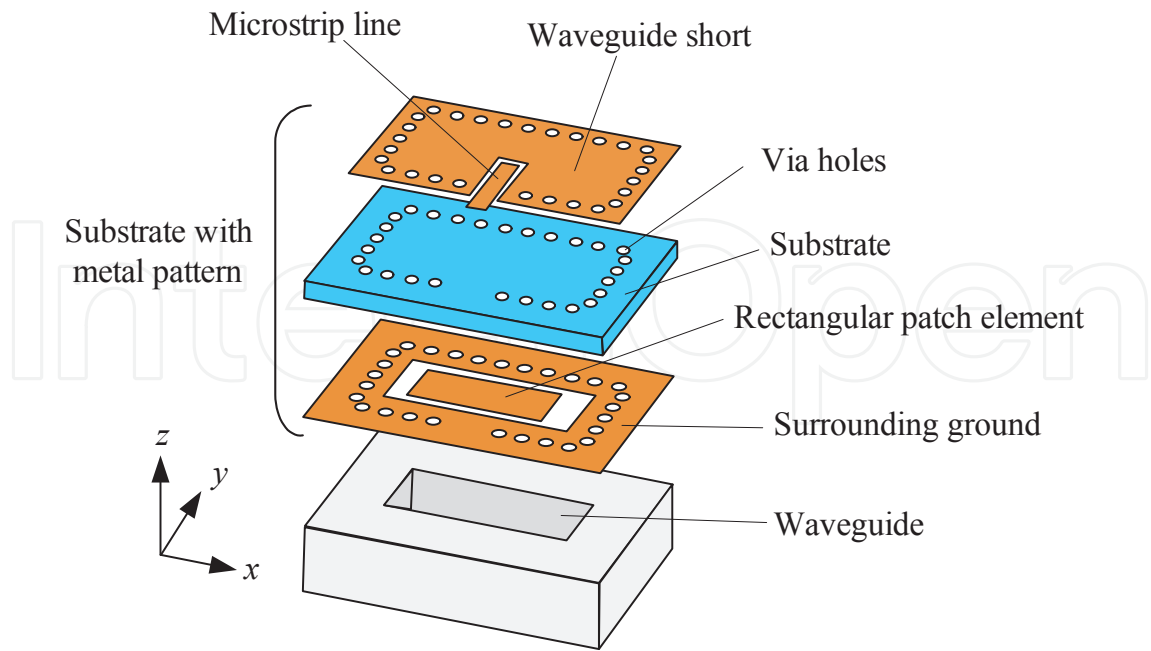


Figure 6. Planar proximity coupling transition

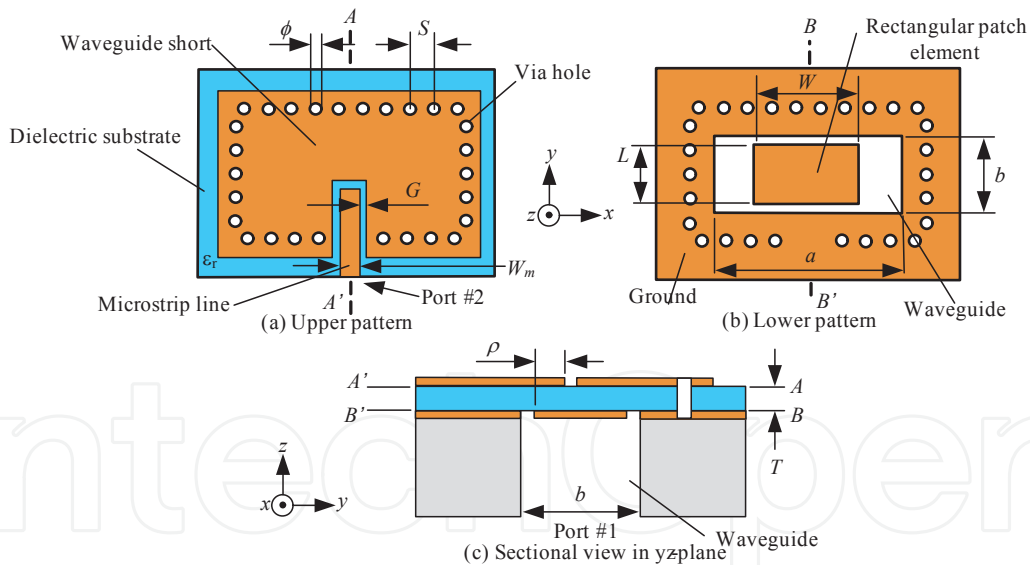


Figure 7. Detailed configuration of planar proximity coupling transition

The microstrip line is inserted into the waveguide and overlaps on the rectangular patch element with overlap length  $\rho = 0.34$  mm. The parameters of the transition are presented in Table 2 for example.

Figure 8 shows the electric field distribution of each mode in  $yz$ -plane. The modes of the microstrip line, the rectangular patch element and the waveguide are quasi TEM transmission

mode,  $TM_{01}$  fundamental resonant mode and  $TE_{10}$  fundamental transmission mode, respectively. Low transmission loss is realized by exchanging quasi TEM transmission mode and  $TE_{10}$  fundamental transmission mode with high efficiency utilizing  $TM_{01}$  fundamental resonant mode. Each parameters in Figure 8 are shown in Table 2 for example.

S-parameters of the reflection  $S_{11}$  and the transmission  $S_{21}$  are calculated by using an electromagnetic simulator based on the finite element method (Ansys HFSS) as shown in Figure 9. From the simulated results, frequency bandwidth of the planar proximity coupling transition is narrow than the ordinary probe transition with back-short.

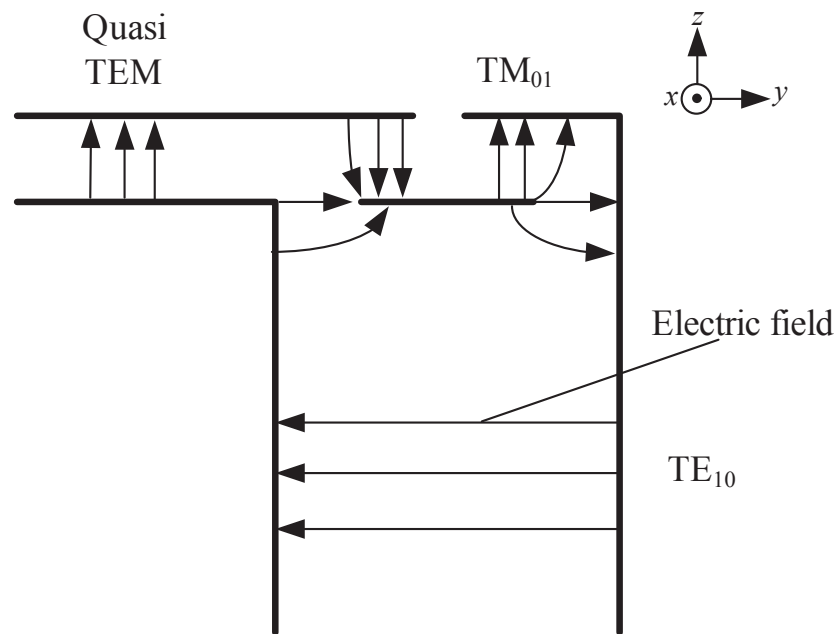


**Figure 8.** Electric field lines of each mode in  $yz$ -plane

Description	Name	Value (mm)	Description	Name	Value (mm)
Broad wall length of waveguide	$a$	3.1	Narrow wall length of waveguide	$b$	1.55
Width of patch element	$W$	2	Length of patch element	$L$	1.1
Width of microstrip line	$W_m$	0.3	Overlap length of inserted probe	$\rho$	0.34
Width of gap	$G$	0.1	Relative permittivity	$\epsilon_r$	2.2
Thickness of substrate	$T$	0.127	Diameter of via hole	$\phi$	0.2
Space between via holes	$S$	0.5			

**Table 2.** Parameters of planar proximity coupling transition

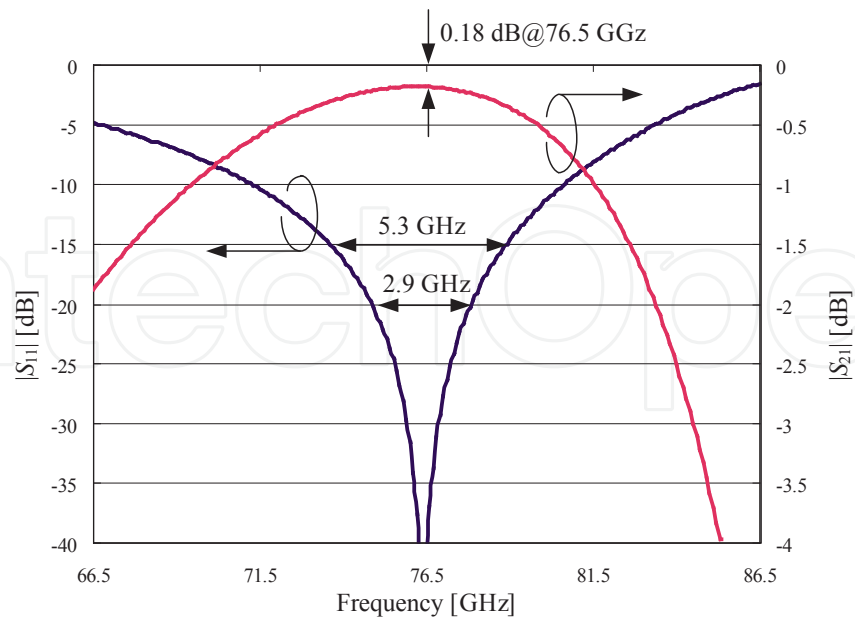


**Figure 9.** Reflection characteristic  $|S_{11}|$  and insertion loss  $|S_{21}|$  of planar proximity coupling transition

### 3.1. Bandwidth of planar proximity coupling transition

The relationships between the parameters and the bandwidth were investigated to specify the optimum parameters for wideband [10]. Figure 10 shows an analytical model that uses a cavity model, which is used for the design of microstrip patch antennas, and the dyadic Green's function of the waveguide.  $L_e$  and  $W_e$  are the effective length and width of the patch element, including the fringing effect.  $t$  and  $\epsilon_e$  are the thickness and the effective relative permittivity of the dielectric substrate. The waveguide dimensions are  $a$  by  $b$ .

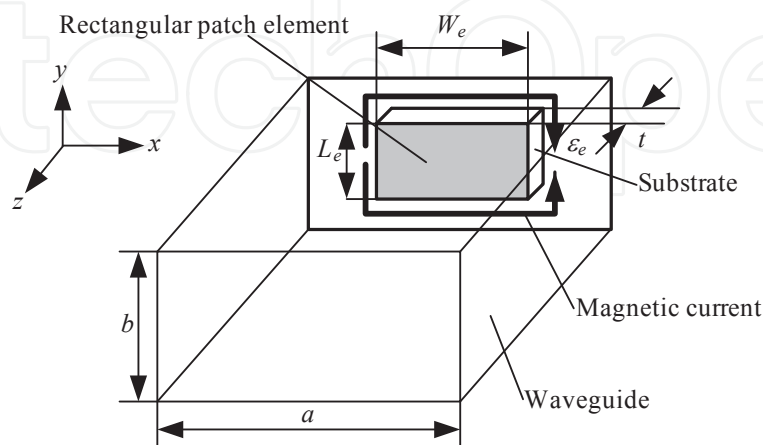


**Figure 10.** Analytical model using cavity model and dyadic Green's function of waveguide

The quality factor  $Q_E$  of the patch element is given by

$$\frac{1}{Q_E} = \frac{1}{Q_{WG}} + \frac{1}{Q_C} + \frac{1}{Q_D} \quad (1)$$

Where,  $Q_{wg}$ ,  $Q_C$ , and  $Q_D$  are quality factors of the power transmitted into the waveguide, conductor loss, and dielectric loss.

The quality factor  $Q_{WG}$  is given with the cavity model and the dyadic Green's function of the waveguide [9] as follows:

$$Q_{WG} = \frac{15\omega\pi\epsilon_0\epsilon_e L_e ab}{2W_e t} \frac{1}{\sqrt{1 - \left(\frac{\lambda_g}{2a}\right)^2}} \frac{1}{\left(\frac{\sin\left(\frac{W_e\pi}{2a}\right)}{\left(\frac{W_e\pi}{2a}\right)}\right)^2} \quad (2)$$

where,  $\omega$ ,  $\epsilon_0$  and  $\lambda_g$  are angular frequency, permittivity in free space, and guided wavelength of waveguide. Relationship between the quality factor  $Q_E$  and the effective width  $W_e$  is solved and the maximum bandwidth is obtained when  $W_e$  is expressed in (3) as follows:

$$W_e = \frac{2ac}{\pi} \quad (3)$$

where,  $C$  is a constant value of 1.666. Equation (3) gives the minimum  $Q$  factor.  $Q_{WG}$  is then given by

$$Q_{WG} \Big|_{W_e = \frac{2aC}{\pi}} = \frac{15\omega\pi^2\epsilon_0\epsilon_e L_e b}{4t} \frac{1}{\sqrt{1 - \left(\frac{\lambda_g}{2a}\right)^2}} \frac{C}{(\sin C)^2} \quad (4)$$

The bandwidth increases with increasing  $a$ , while the effective width  $W_e$  is set to the optimum width for wideband.

The relationships between the parameters and the bandwidth are summarized in Table 3.

Parameters		Bandwidth
Effective width $W_e$ of patch element	$W_e = 2aC/\pi$	Max.
Broad wall length $a$ of waveguide	↗	↗
Narrow wall length $b$ of waveguide	↘	↗
Effective relative permittivity $\epsilon_e$	↘	↗
Thickness of substrate $t$	↗	↗
Effective length $L_e$ of patch element	$\lambda_e/2$	—

**Table 3.** Relations between parameters and bandwidth

## 4. Broadband microstrip-to-waveguide transition

This section presents broadband techniques of the proximity coupling type transition. Refer to the 79 GHz UWB applications, 4 GHz bandwidth is required [12]. The proximity coupling type transition has bandwidth of 6.9 % (5.29 GHz) for the reflection coefficient below -15 dB [10]. Considering the tolerance for the manufacturing accuracy, much wider bandwidth is required. The broadband transition was presented using waveguide with large broad-wall [13]. Maximum width of the waveguide where higher order mode does not propagate is applied and the distance from the edge of broad-wall of the waveguide to via holes on the broad-wall side of the waveguide is examined to have optimum length for wideband.

### 4.1. Transition structure

Configuration of the transition is shown in Figure 11 and Figure 12. A microstrip line, a probe and a waveguide short are located on the upper plane of the dielectric substrate. A rectangular patch element and a surrounding ground are patterned on the lower plane of the dielectric substrate. Via holes surround the aperture of the waveguide on the lower plane of the dielectric substrate to connect the surrounding ground and the waveguide short electrically. The required operation bandwidth is from 77 GHz to 81 GHz.

In terms of the bandwidth, it becomes wider as broad-wall length  $a$  of the waveguide increases, and narrow-wall length  $b$  of the waveguide decreases [10]. First, standard waveguide WR-10 can be applied for dominant mode propagation at the design frequency (79 GHz). Therefore narrow-wall length  $b$  of the waveguide is determined to be 1.27 mm which is the same as the narrow-wall length of WR-10 standard waveguide.

Next, the broad-wall length  $a$  of the waveguide is increased as large as possible to 3.1 mm where higher order mode in the waveguide does not propagate. A rectangular patch element with the width  $W = 2.26$  mm and the length  $L = 0.98$  mm is located on the lower plane of the dielectric substrate at the center of the waveguide. The width  $W_m$  of the microstrip line is 0.3 mm corresponding to approximately 56 ohm of characteristic impedance. The probe with the width  $W_p = 0.35$  mm is inserted into the waveguide and overlaps on the rectangular patch element with length  $\rho = 0.32$  mm. The distance from the edge of broad-wall of the waveguide to via holes on the broad-wall side  $V_y$  is 0.46 mm. The distance from the edge of narrow-wall of the waveguide to via holes on the narrow-wall side  $V_x$  is 0.4 mm. The thickness of dielectric substrate  $T$  is 0.127 mm with relative permittivity  $\epsilon_r$  is 2.2. The parameters of the transition are presented in Table 4.

### 4.2. Design and numerical investigation

The transition is investigated numerically by using the electromagnetic simulator based on the finite-element method (Ansys HFSS). In this calculation, loss tangent  $\tan\delta = 0.001$  and conductivity  $\sigma = 5.8 \times 10^7$  S/m of a copper clad are used as loss factors. The reflection characteristic  $|S_{11}|$  and the insertion loss  $|S_{21}|$  of the transition with parameters in Table 4 are presented in Figure 13.

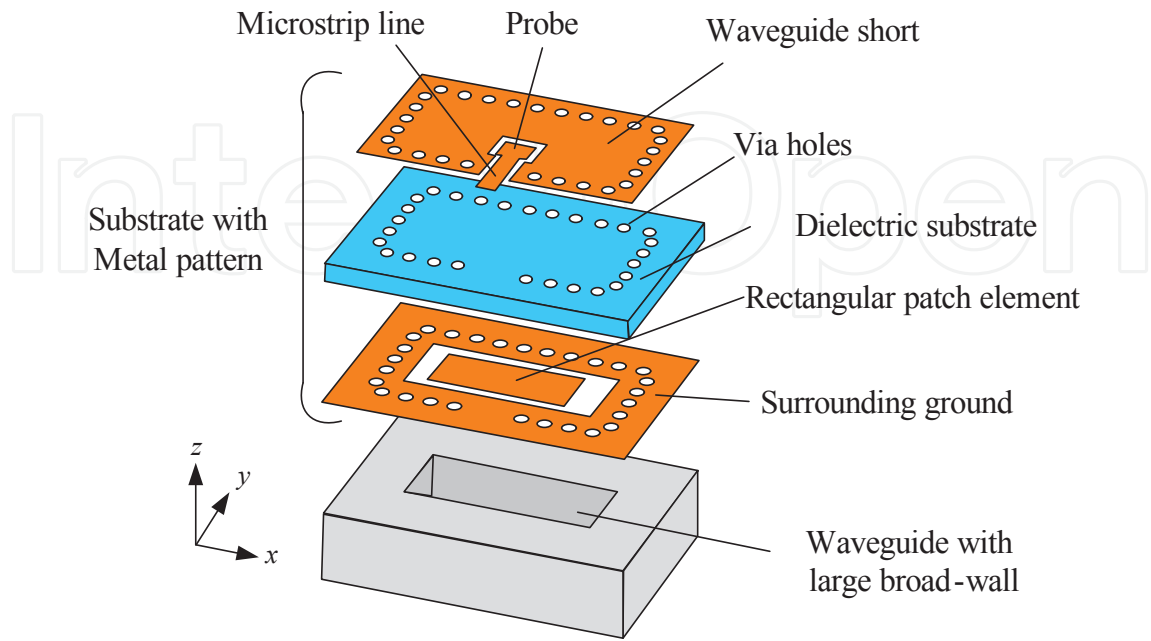


**Figure 11.** Configuration of broadband transition

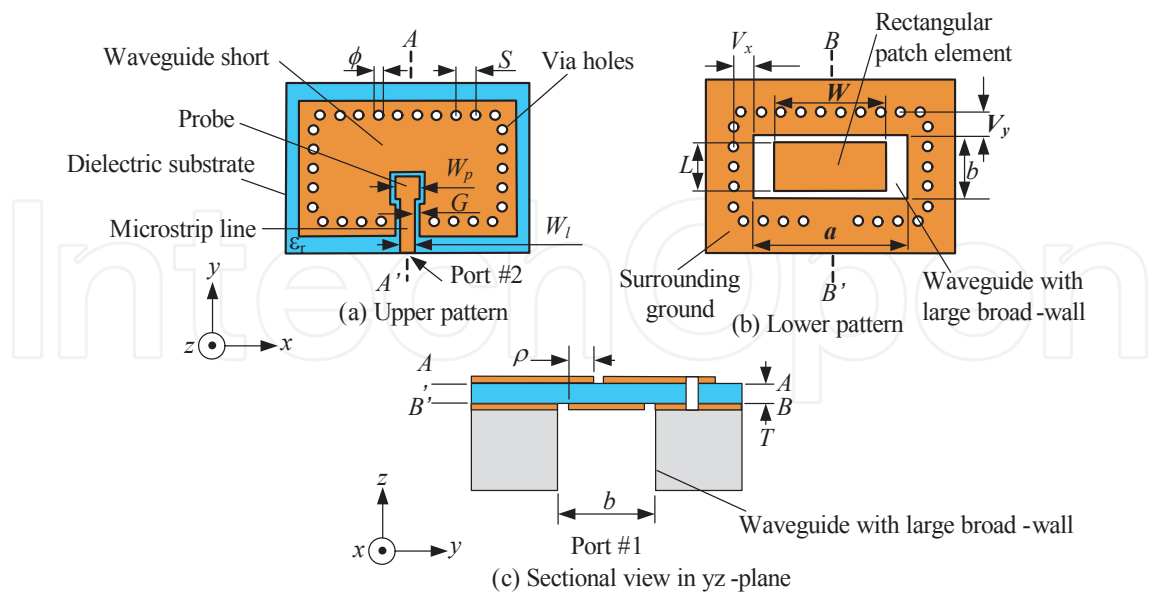


**Figure 12.** Detailed configuration of broadband transition

Description	Name	Value (mm)	Description	Name	Value (mm)
Broad wall length of waveguide	$a$	3.1	Narrow wall length of waveguide	$b$	1.27
Width of patch element	$W$	2.26	Length of patch element	$L$	0.98
Width of microstrip line	$W_m$	0.3	Width of probe	$W_p$	0.35
Overlap length of inserted probe	$\rho$	0.32	Width of gap	$G$	0.1
Thickness of substrate	$T$	0.127	Relative permittivity	$\epsilon_r$	2.2
Space between via holes	$S$	0.4	Diameter of via hole	$\phi$	0.2
Distance from broad wall to via hole	$V_y$	0.46	Distance from narrow wall to via hole	$V_x$	0.4

**Table 4.** Parameters of the broadband transition

It can be seen from the simulation results that the bandwidth for the reflection coefficient  $|S_{11}|$  below -15 dB is 14.4 GHz, and the insertion loss  $|S_{21}|$  is -0.28 dB from 77 GHz to 81 GHz. In this case, two different resonances are observed. Lower resonant frequency is 76.4 GHz and higher resonant frequency is 85.5 GHz.

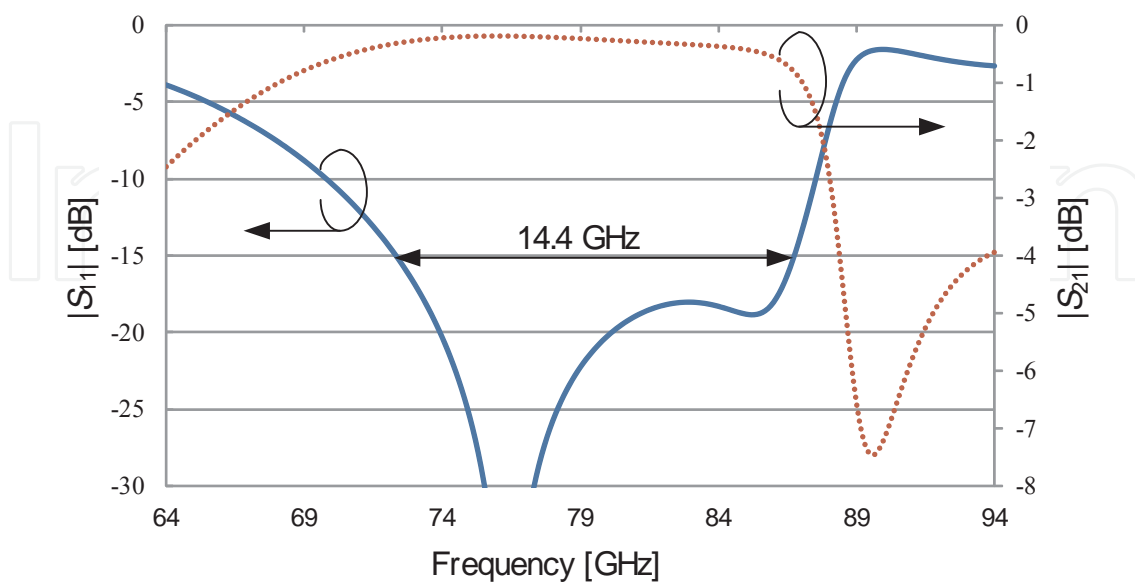


**Figure 13.** Reflection characteristic  $|S_{11}|$  and insertion loss  $|S_{21}|$  of broadband transition

Figure 14 shows the calculated electric field distributions in the  $xy$ -plane including  $BB'$ -line at 76.4 GHz, 79 GHz and 85.5 GHz. It is observed that fundamental mode of  $TM_{01}$  is excited at 76.4 GHz and 79 GHz in Figure 14 (a) and (b). On the other hand, a higher order mode is observed at 85.5 GHz as shown in Figure 14 (c).

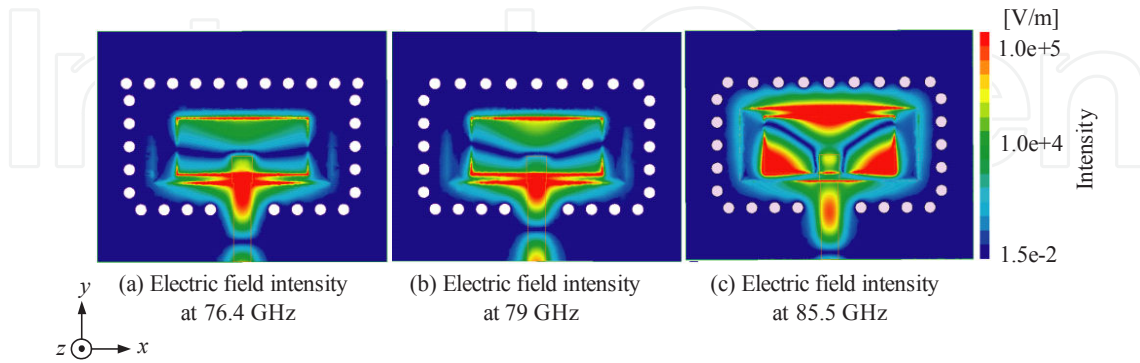


**Figure 14.** Electric field intensity distributions in  $xy$ -plane.

#### 4.2.1. Lower operation frequency by $L$

The length  $L$  of the rectangular patch element affects to the lower resonant frequency as shown in Figure 15. The lower resonant frequency can be controlled by the length  $L$  of the rectangular patch element.

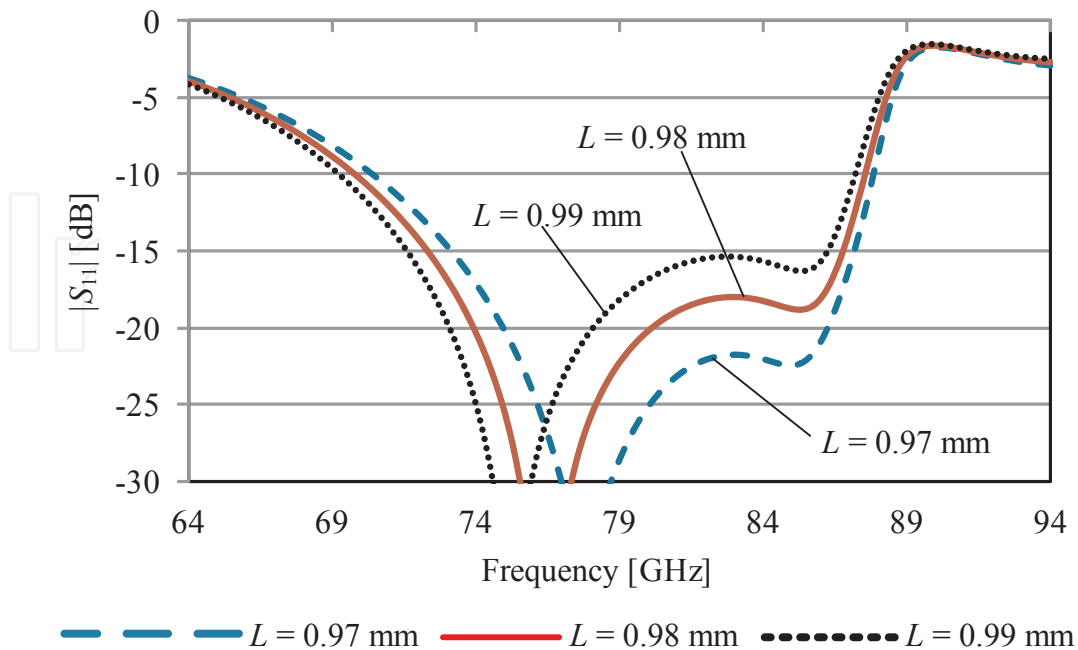


**Figure 15.**  $|S_{11}|$  vs. length  $L$  of the patch element (Lower resonant frequency control)

#### 4.2.2. Higher operation frequency by $V_y$

The distance  $V_y$  from the edge of the broad-wall of the waveguide to via holes affects to the higher resonant frequency as shown in Figure 16. The higher resonant frequency can be controlled by the distance  $V_y$  from the edge of the broad-wall of the waveguide to via holes.

IntechOpen

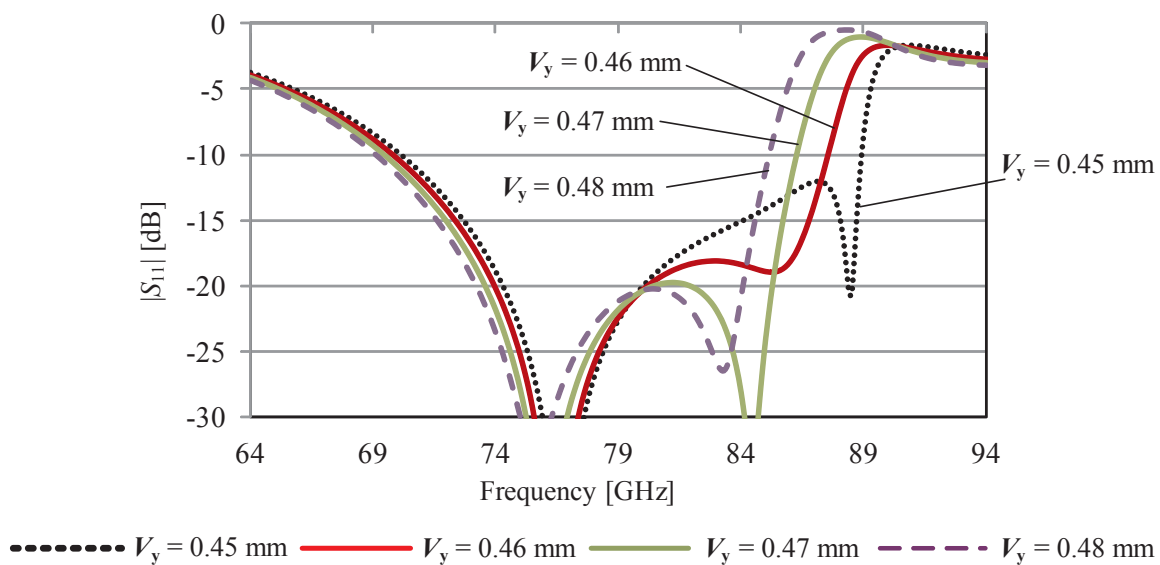


**Figure 16.**  $|S_{11}|$  vs. distance  $V_y$  from the edge of the broad-wall of the waveguide to via holes (Higher resonant frequency control)

IntechOpen

#### 4.2.3. Impedance matching by $\rho$ and $W_p$

The overlap length  $\rho$  of the inserted probe is most effective for the impedance matching to the waveguide as shown in Figure 17. Increment of the overlap length  $\rho$  of the inserted probe with rectangular patch element causes increase of inductance.

The width  $W_p$  of the probe is also effective for the impedance matching to the waveguide as shown in Figure 18. Increment of width  $W_p$  of the probe causes decrease of resistance. These Smith charts are observed from the waveguide *port#1* in Figure 12 (c) at a distance of 2.0 mm under the surrounding ground on the lower plane of the substrate.

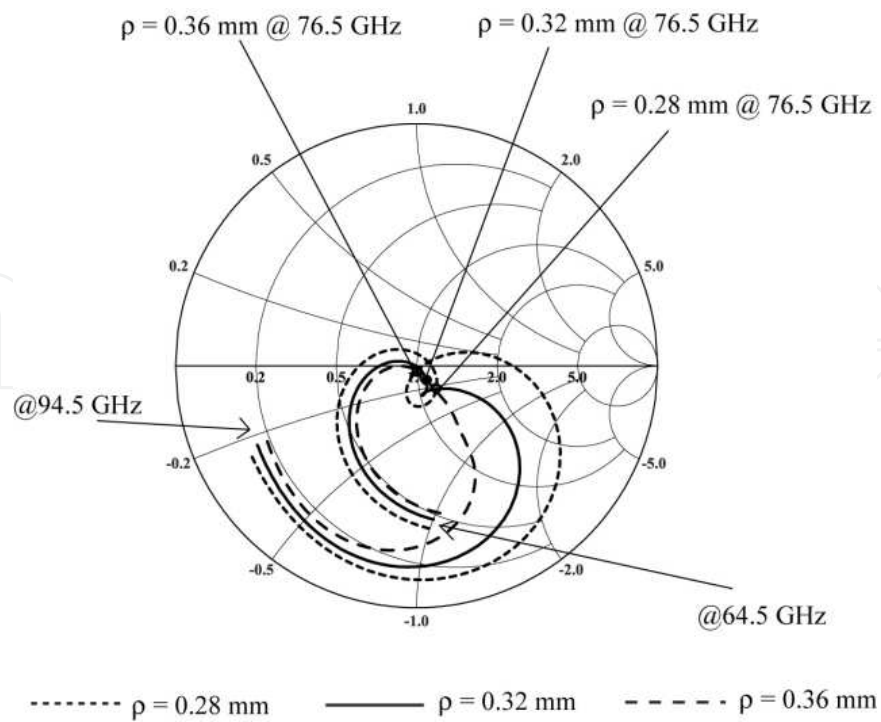


**Figure 17.** Impedance vs. overlap length  $\rho$  of the inserted probe

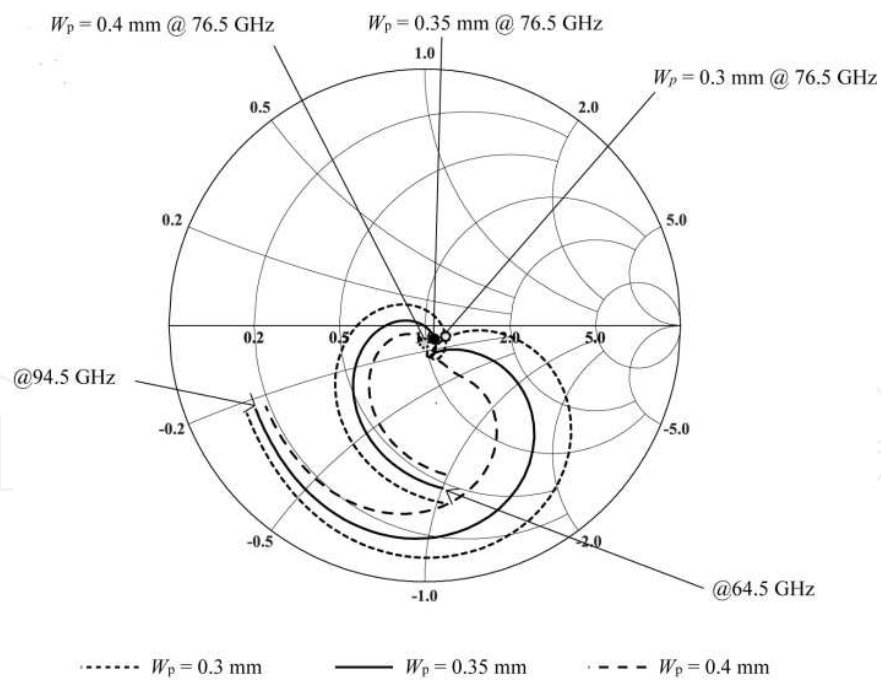


**Figure 18.** Impedance vs. width  $W_p$  of the probe

So, the impedance matching can be controlled by optimizing of the overlap length  $\rho$  of inserted probe and the width  $W_p$  of the prove.

#### 4.2.4. Wideband impedance matching by $\rho$ and $W_p$

For the wideband impedance matching, both of the length  $\rho$  of the inserted probe and the width  $W_p$  of the probe are optimized as shown in Figure 19. It can be seen from the simulation results that both of  $\rho$  and  $W_p$  affect the wideband impedance matching. In these design, other parameters except  $\rho$  and  $W_p$  are same as in Table 4.

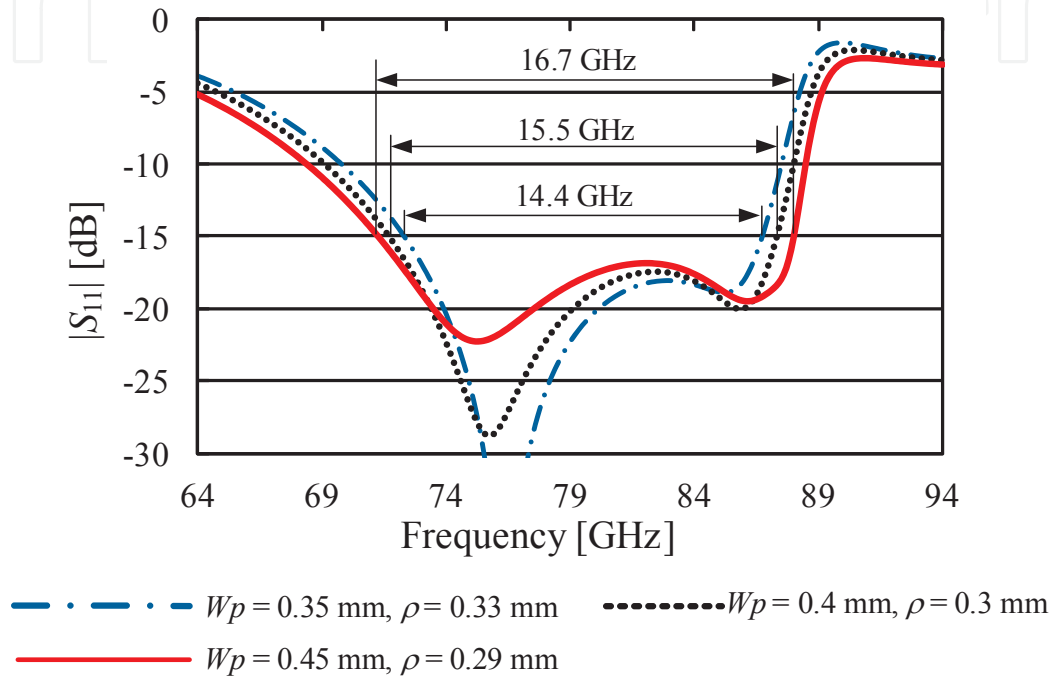


**Figure 19.** Comparison of three type transitions

### 4.3. Experiment

Three transitions for the results shown in Figure 19 are fabricated. The photograph of the fabricated transitions are in Figure 20. Figure 20 (a) shows the upper plane of the substrate and is common for each design except the width  $W_p$  of the probe and the overlap length  $\rho$  of the inserted probe as each design. Figure 20 (b) shows the lower plane of the substrate and is common at each design.

#### 4.3.1. Measured bandwidth

Measured the reflection coefficient are shown in Figure 21. Maximum bandwidth for reflection coefficients below -15 dB is 15.1 GHz when  $W_p$  is 0.45 mm and  $\rho$  is 0.29 mm. In this measurement, the device-under-test (DUT) was composed of a pair of transitions with one microstrip line between them as shown in Figure 21. The measured  $|S_{11}|$  and  $|S_{21}|$  in Figure 22 were given by taking the transmission coefficient of the DUT, subtracting the loss of the microstrip line, and dividing by two. The loss of the microstrip line was measured as 0.05 dB/mm from 77 GHz

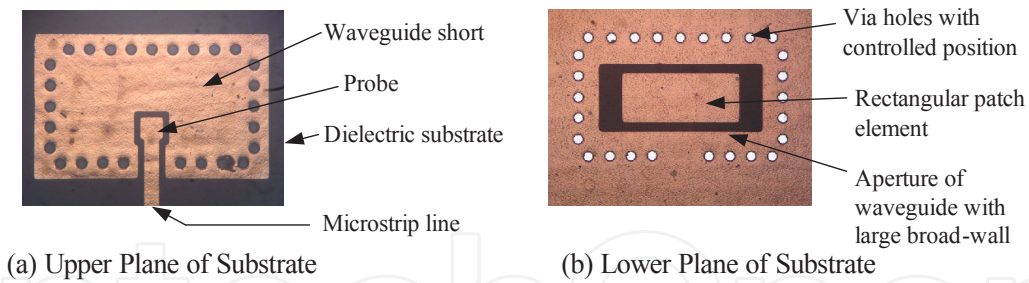


**Figure 20.** Fabricated transitions

to 81 GHz. A time gate function was used to exclude undesired waves, and high accuracy was achieved in this measurement. The distance between the center of the waveguides was set at 50 mm, which was long enough to distinguish between desired and undesired waves in the time domain.

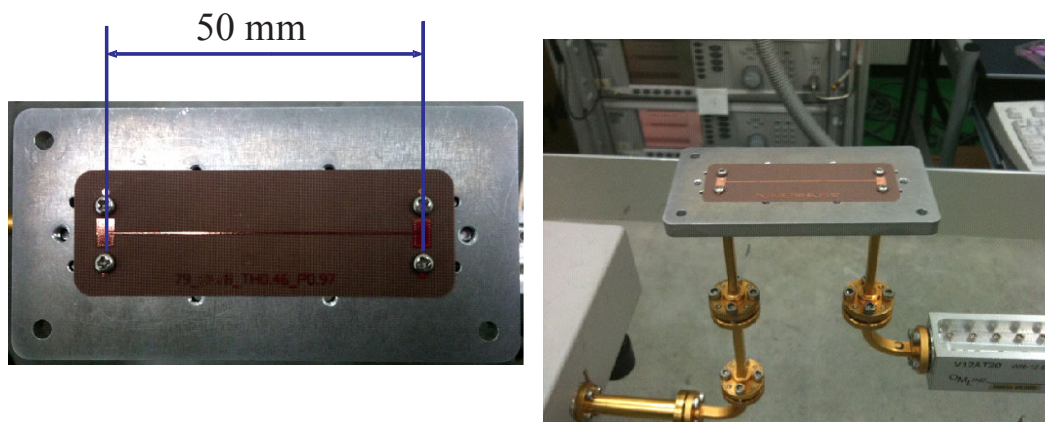


**Figure 21.** DUT in measurement

#### 4.3.2. Comparison of measured performance

Figure 23 shows the comparison of three designed transitions. Refer to the bandwidth, measured results are approximately 1.8 GHz decreased compared with the simulation results. For the insertion loss, the measured results are approximately 0.38 dB increased compared with the simulation results.

In these results, design of increased bandwidth causes increase of insertion loss. Therefore, the bandwidth and the insertion loss is in tradeoff relation. So, the transition required each application can be designed by optimizing of each parameters.

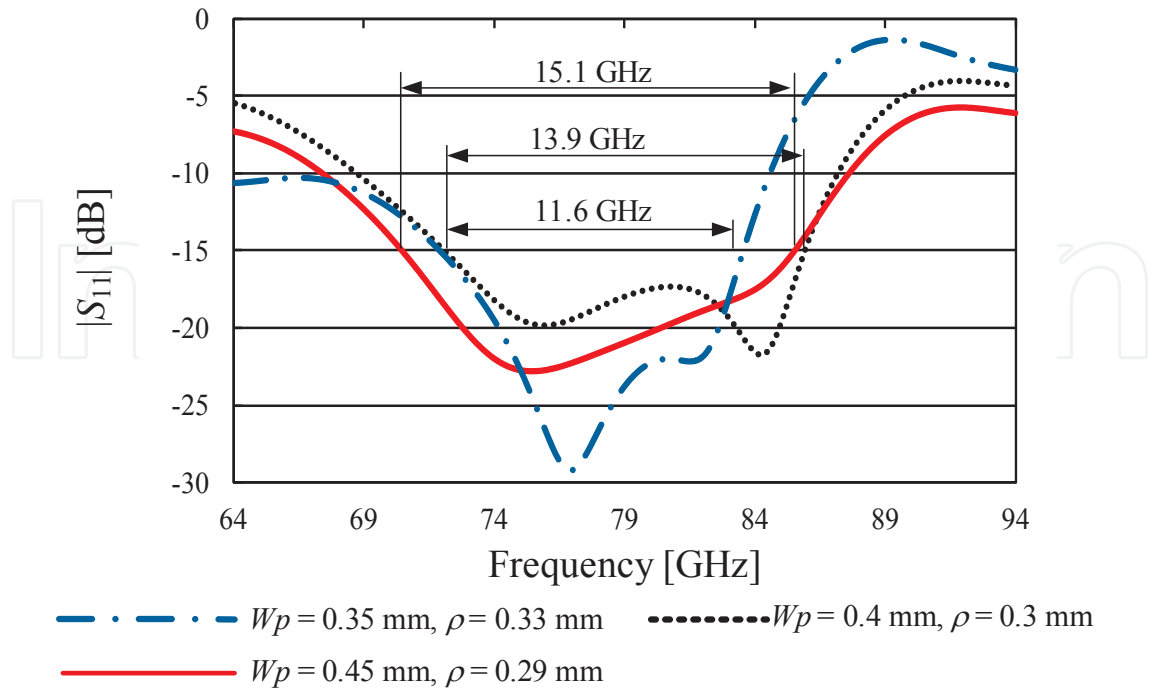


Figure 22. Measured bandwidth of three type transitions

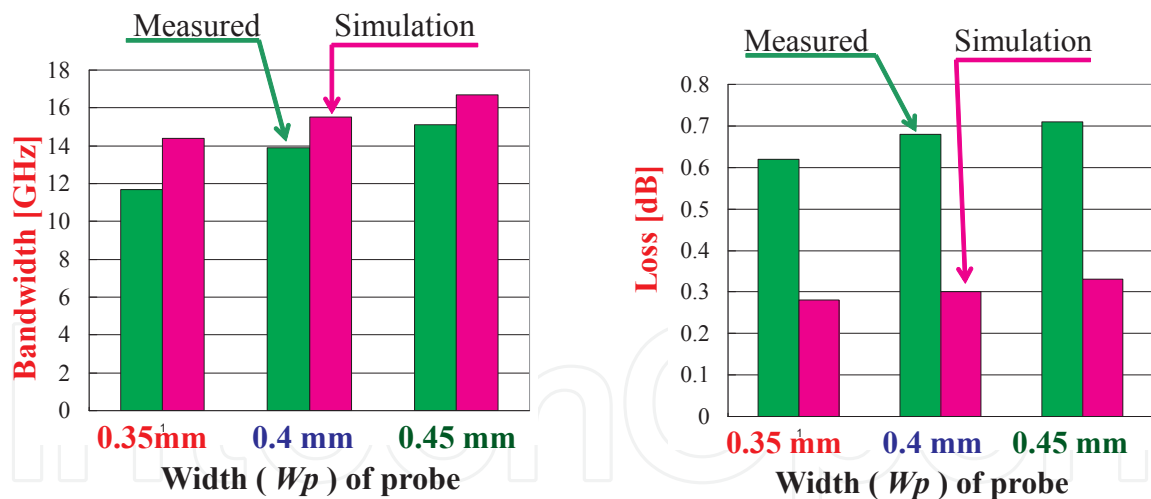


Figure 23. Comparison of measured performance

#### 4.4. Conclusion

Broadband microstrip-to-waveguide transition using waveguide with large broad-wall were developed in millimeter-wave band. By applying large broad-wall, the bandwidth is extended. Moreover, the distance from the edge of the broad-wall of the waveguide to via holes are examined to create double resonances, consequently the bandwidth is extended.

Three types of design are presented. It is confirmed by experiments that the most wideband transition exhibits a bandwidth of 19.1 % (15.1 GHz) for the reflection coefficient below -15 dB and insertion loss of -0.71 dB from 77 GHz to 81 GHz.

## 5. Narrow-wall-connected microstrip-to-waveguide transition

Narrow-wall-connected microstrip-to-waveguide transition using V-shaped patch element in millimeter-wave band was proposed [14]. Since the microstrip line on the narrow-wall is perpendicular to the  $E$ -plane of the waveguide, the waveguide field does not couple directly to the microstrip line. The current on the V-shaped patch element flows along the inclined edges, then current on the V-shaped patch element couples to the microstrip line efficiently. Three types of the transitions are investigated.  $S$ -parameters of the reflection  $S_{11}$  and the transmission  $S_{21}$  are calculated by using an electromagnetic simulator based on the finite element method (Ansys HFSS). The numerical investigations of these transitions show some relations between the bandwidth and the insertion loss. It is confirmed that the improved transition exhibits an insertion loss of 0.6 dB from 76 to 77 GHz, and a bandwidth of 4.1 % (3.15 GHz) for the reflection coefficient below -15 dB.

### 5.1. Background

In some applications, narrow-wall-connected micro-strip-to-waveguide transition is required. Refer to the former developed proximity coupling type transition [9],[10], the microstrip line is located on the waveguide broad-wall and the microstrip line probe is parallel to  $E$ -plane of the waveguide, therefore, current on the rectangular patch element couples to the microstrip line efficiently. However, on the occasion of the microstrip line on the narrow-wall of the waveguide, the microstrip line probe is orthogonal to  $E$ -plane of the waveguide. Therefore, they do not couple essentially. To couple currents on the microstrip line and the patch element, a V-shaped patch element is applied instead of the rectangular patch element.

### 5.2. Transition structure and design

#### 5.2.1. Transition structure

Configuration of the transition is shown in Figure 24 and Figure 25. The microstrip line and the waveguide short are located on the upper plane of the dielectric substrate. The V-shaped patch element and the surrounding ground are patterned on the lower plane of the dielectric substrate. Via holes are surrounding the aperture of the waveguide on the lower plane of the substrate to connect the surrounding ground and the waveguide short electrically. The design frequency range is from 76 GHz to 77 GHz. The V-shaped patch element is designed as follows. Refer to the conventional proximity coupling type [9],[10], the current on rectangular patch element has only  $y$ -component which is parallel to  $E$ -plane of the waveguide shown in Figure 26 (a). In this case, the current on the rectangular patch element is parallel to the microstrip line, therefore, the current on the rectangular patch element couples to the microstrip line. On

the other hand, current on the patch element which is excited by electromagnetic field in the waveguide must have both of  $x$ -component and  $y$ -component in order to couple to the microstrip line on the waveguide narrow-wall. The current on the V-shaped patch element is divided to two directions along the side edge as shown in Figure 26 (b). Consequently, the current on the V-shaped patch element creates parallel component with the microstrip line, and effective coupling is achieved with the microstrip line.

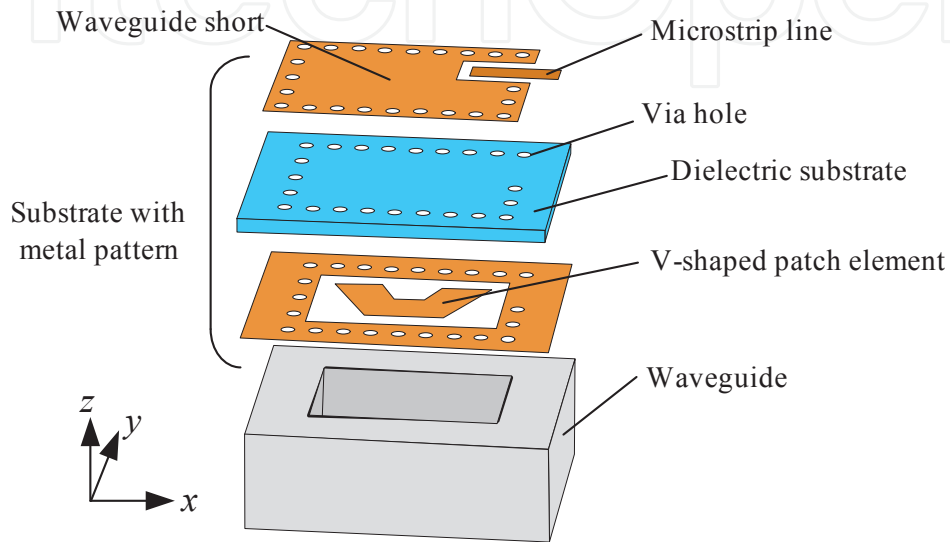


Figure 24. Configuration of transition

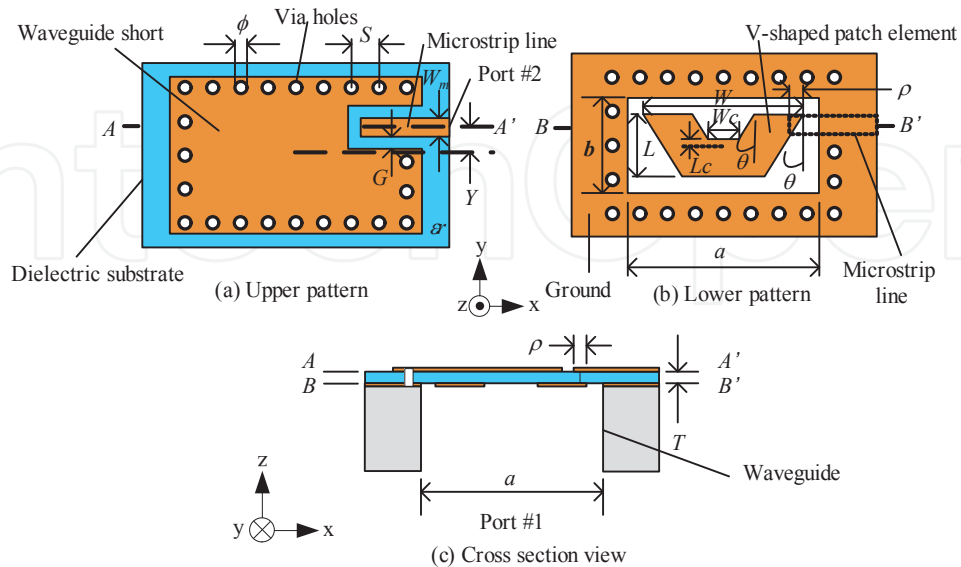
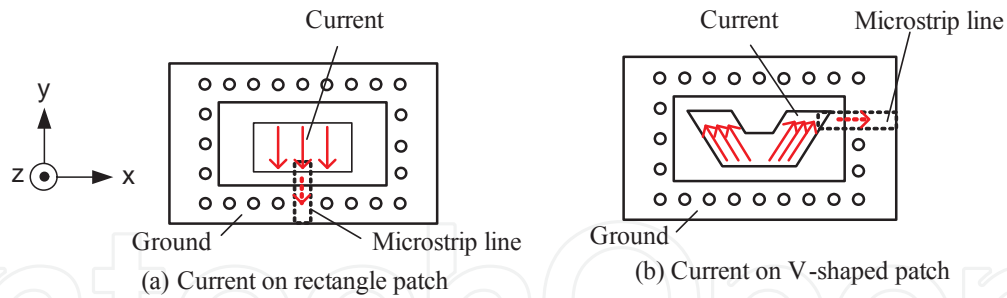


Figure 25. Detailed configurations of transition



**Figure 26.** Current distributions on patch element

### 5.2.2. Transition design

First, the rectangular patch element with the width  $W = 2.6$  mm and the length  $L = 1.02$  mm is located on the lower plane of the dielectric substrate at the center of the waveguide. Then, both sides of the rectangular patch element are cut by the patch-cut-angle  $\theta = 30$  degrees and also middle of upper horizontal edge of the rectangular patch element is cut as shown in Figure 25 (b). The microstrip line is located on the waveguide narrow-wall as shown in Figure 25 (a) with the shift length  $Y = 0.34$  mm from the center of the waveguide. The microstrip line is located just above the side edge of the V-shaped patch element as shown in Figure 25 (b). The microstrip line is inserted into the waveguide and overlaps over the V-shaped patch element with the length  $\rho = 0.23$  mm. The parameters of the transition are presented in Table 5.

Mode conversion from the waveguide to the microstrip line is achieved by the resonance of the V-shaped patch element. The dominant  $TE_{10}$  mode of the waveguide is converted to the quasi-TEM mode of the microstrip line. Figure 27 shows the calculated electric field intensity distribution in the  $xy$ -plane including  $BB'$ -line. The electric field intensity  $E$  includes  $x, y$  and  $z$  components of the electric field. The V-shaped patch element is resonated in two directions, by the resonance of current distribution along the both side edges of the V-shaped patch element.

Description	Name	Value (mm)	Description	Name	Value (mm)
Width of patch element	$W$	2.6	Width of gap	$G$	0.1
Length of patch element	$L$	1.02	Thickness of substrate	$T$	0.127
Patch cut angle	$\theta$	30 deg.	Relative permittivity	$\epsilon_r$	2.2
Overlap length of inserted microstrip line	$\rho$	0.23	Broad wall length of waveguide	$a$	3.1
Width of cut patch element	$W_c$	0.46	Narrow wall length of waveguide	$b$	1.55
Length of cut patch element	$L_c$	0.1	Diameter of via hole	$\phi$	0.2
Width of microstrip line	$W_m$	0.3	Space between via holes	$S$	0.5
Shift length of microstrip line from center of waveguide	$Y$	0.34			

**Table 5.** Parameters of transition

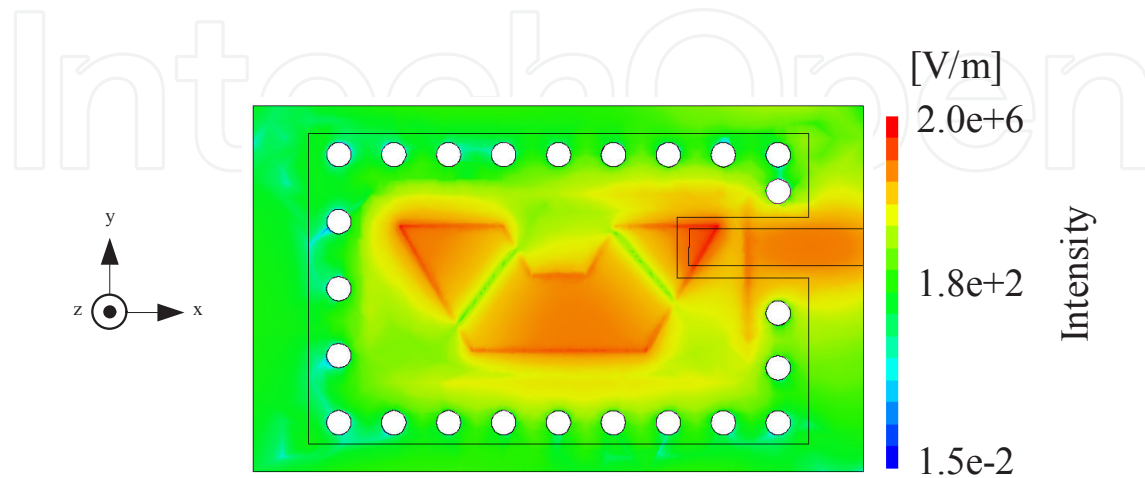


**Figure 27.** Electric field intensity distribution in  $xy$ -plane

### 5.3. Numerical investigation

#### 5.3.1. Operating frequency by $L$

The reflection characteristic of the V-shaped patch element with the length  $L = 1.02$  mm is presented in Figure 28. It can be seen from the simulation results that the bandwidth for  $|S_{11}|$  below  $-15$  dB is 2 GHz, and the insertion loss  $|S_{21}|$  is 0.32 dB over the frequency range from 76 GHz to 77 GHz. The length  $L$  of the V-shaped patch element affects to the resonant frequency as shown in Figure 28. Increment of the length  $L$  of the V-shaped patch element causes the lower resonant frequency. So, operating frequency of this transition can be controlled by the length  $L$  of the V-shaped patch element.

#### 5.3.2. Impedance matching by $\rho$

The overlap length  $\rho$  of the inserted microstrip line affects to the impedance as shown in Figure 29. Increment of the overlap length  $\rho$  causes increases of capacitive reactance at the desired frequency, and decrement of the overlap length  $\rho$  causes increases of inductive reactance. This Smith chart is observed from the waveguide *port#1* in Figure 25 (c) at a distance of 1.5 mm under the surrounding ground on the lower plane of the substrate. So, impedance matching can be controlled by adjusting the overlap length  $\rho$  to cancel reactive component.

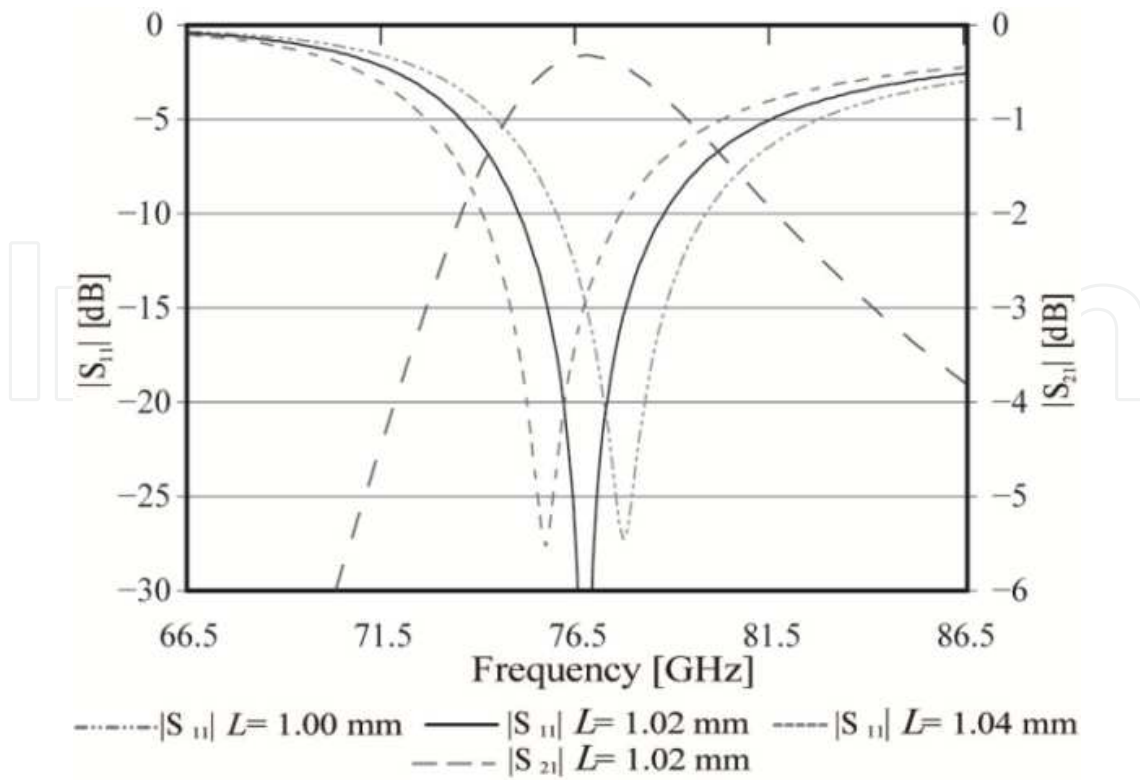


Figure 28.  $|S_{11}|$  vs. length of V-shaped patch element  $L$  and transition characteristic  $|S_{21}|$

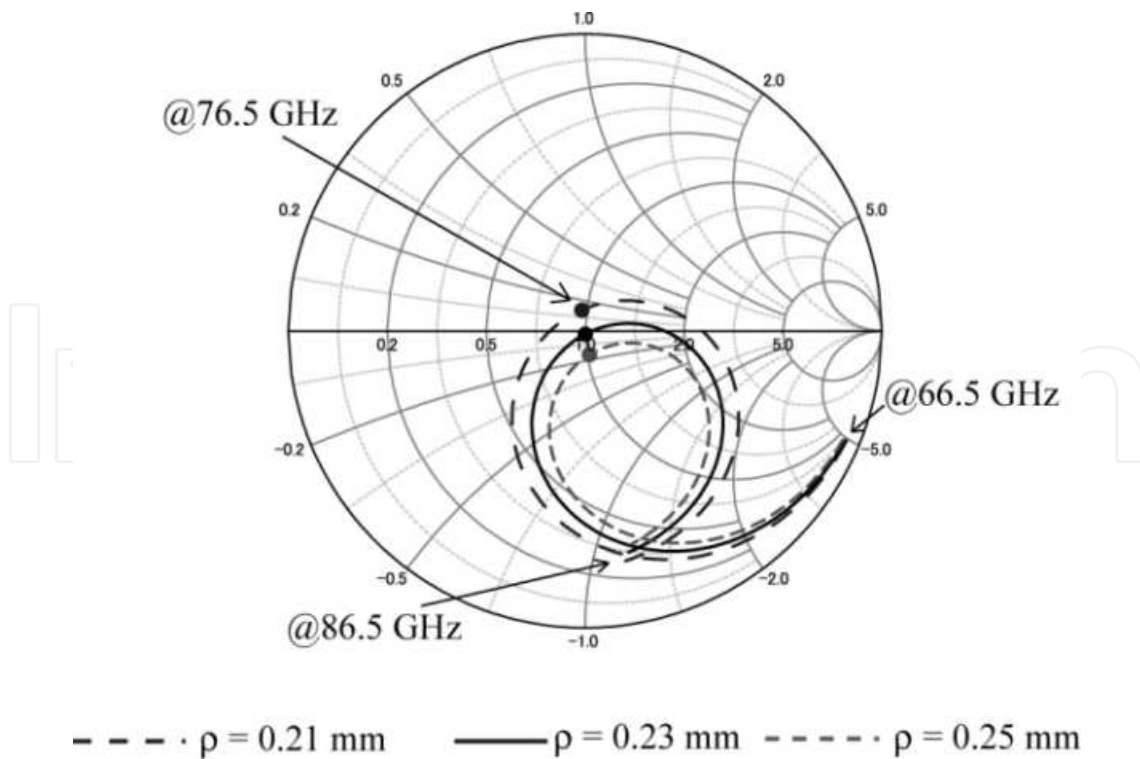
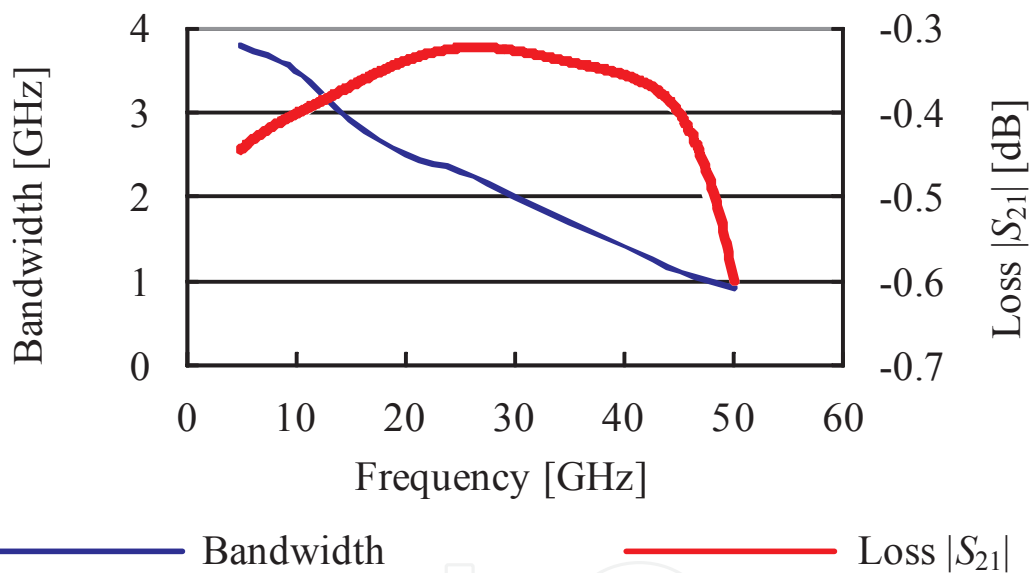


Figure 29. Relation between Impedance and Length of Inserted Microstrip Line  $\rho$  from 66.5 GHz to 76.5 GHz

### 5.3.3. Bandwidth by $\theta$

The patch cut angle  $\theta$  affects to the bandwidth for the reflection coefficient below -15 dB as shown in Figure 30. The transition characteristic change is investigated by change of the patch cut angle  $\theta$  from 5 degrees to 50 degrees. Some parameters of  $W, L, \rho, W_c, L_c$  and  $Y$  are optimized at each patch cut angle  $\theta$ . Least insertion loss  $|S_{21}|$  is obtained at 30 degrees of the patch cut angle  $\theta$ . In this case, the bandwidth for  $|S_{11}|$  below -15 dB is 2 GHz and the insertion loss  $|S_{21}|$  is -0.32 dB.

On the occasion of the patch cut angle  $\theta = 10$  degrees, the bandwidth is extended to 3.5 GHz, but the insertion loss  $|S_{21}|$  is increased to -0.41 dB compared with the patch cut angle  $\theta = 30$  deg.



**Figure 30.** Bandwidth and transition characteristic  $|S_{21}|$  related by patch cut angle  $\theta$

In the design with the small patch cut angle  $\theta$ , current on the V-shaped patch element has small  $x$ -component, therefore the loss increases. The cause is that the magnetic field is small. This magnetic field is excited by the current of  $x$ -component on the V-shaped patch element and the magnetic field surrounds the microstrip line. Small magnetic field causes weak coupling between the V-shaped patch element and the microstrip line. Figure 4.31 shows calculated magnetic field distribution in the  $yz$ -plane at the  $x$  position of 2.48 mm. The magnetic field intensity  $H$  include  $x, y$  and  $z$  components of the magnetic field. On the other hand, in the design with large patch cut angle  $\theta$ , the area of the V-shaped patch element decreases and the quality factor  $Q$  of the patch element increases, then bandwidth decreases.

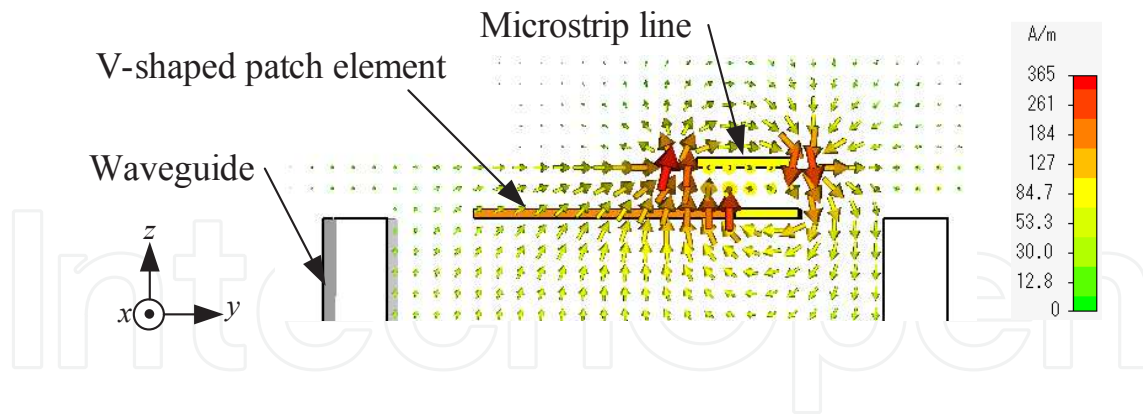


**Figure 31.** Magnetic field distribution in yz-plane at  $x = 2.48$  mm

## 5.4. Design variety of transition

### 5.4.1. Low loss design

As shown in Figure 30, least insertion loss is obtained at the patch cut angle  $\theta = 30$  degrees. Configuration is shown in Figure 25 and design parameters are just the same as shown in Table 5. The bandwidth for  $|S_{11}|$  below -15 dB is 2 GHz and the insertion loss  $|S_{21}|$  is -0.32 dB.

### 5.4.2. Wideband design

In this design, the patch cut angle  $\theta$  of 10 degrees is applied. Configuration is shown in Figure 30 and some parameters must be changed as Table 6, but other parameters are the same as Table 5. Characteristic of this transition is shown in Figure 4.13. The bandwidth for  $|S_{11}|$  below -15 dB is 3.5 GHz and the insertion loss  $|S_{21}|$  is -0.41 dB.

Description	Name	Value (mm)
Length of patch element	$L$	1.11
Patch cut angle	$\theta$	10 deg.
Overlap length of inserted microstrip line	$\rho$	0.28
Width of cut patch element	$W_c$	0.5
Shift length of microstrip line from center of waveguide	$Y$	0.385

**Table 6.** Parameters of wideband design

### 5.4.3. Wideband and low loss design

The transition with the wideband design described before is modified. At the  $y$ -directional position  $C_y = 0.32$  mm from the top of the V-shaped patch element, the V-shape patch element is cut to  $x$ -direction with the length  $C_x$  of 0.1mm as shown in Figure 32. The basic configuration

is as shown in Figure 25 but the V-shaped patch element is modified as shown in Figure 32. Some parameters are optimized and changed as Table 7, although other parameters are the same as Table 5.

To get the wideband of the transition, the patch cut angle  $\theta$  is kept to 10 degrees. To achieve strong coupling, this modification of V-shaped patch element is effective. Due to this structural modification, horizontal component of electric current on the patch element increases. Consequently strong coupling to the microstrip line is achieved. The bandwidth for  $|S_{11}|$  below -15 dB is 3.1 GHz and the insertion loss  $|S_{21}|$  is 0.34 dB. The bandwidth is 0.4 GHz narrow than the wideband design and the loss is approximately equal as the low loss design.

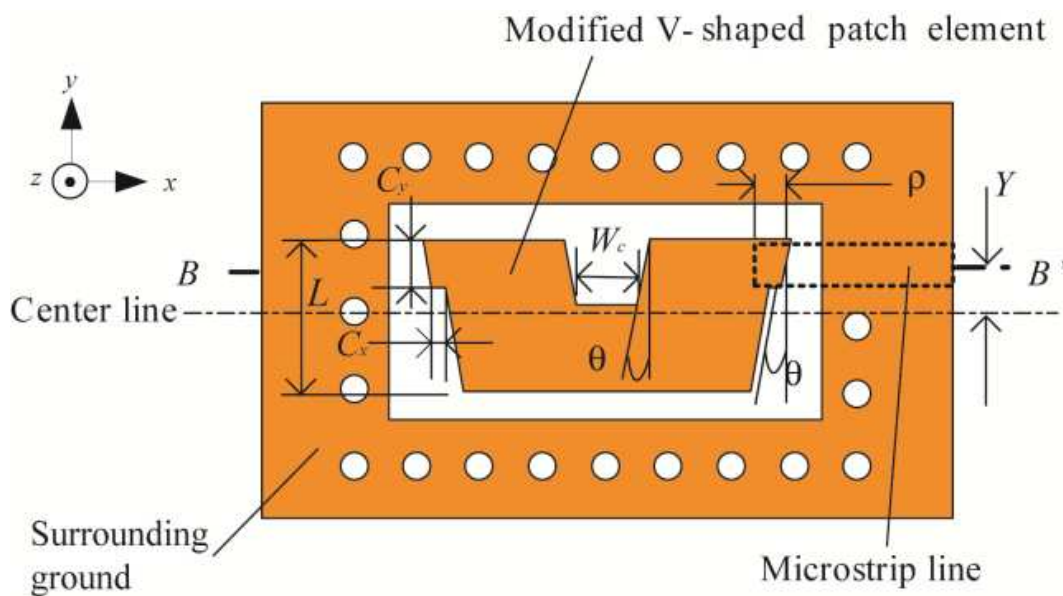


**Figure 32.** Lower pattern of the transition with modified V-shaped patch element

Description	Name	Value (mm)
Cut length in x-direction	$C_x$	0.1
Cut length in y-direction	$C_y$	0.32
Length of patch element	$L$	1.08
Patch cut angle	$\theta$	10 deg.
Overlap length of inserted microstrip line	$\rho$	0.27
Width of cut patch element	$W_c$	0.45
Shift length of microstrip line from center of waveguide	$Y$	0.37

**Table 7.** Parameters of wideband and low loss design

### 5.5. Measured performance of three transitons

The photograph of the fabricated transitions are shown in Figure 33. Figure 33 (a) shows the upper plane of the substrate and is common for each design except  $y$ -position of the microstrip line( $Y$ ). As described before, the shift length  $Y$  of the microstrip line from the center of the waveguide is changed at each design. Figure 34 shows the comparison of three designed transitions. Refer to the bandwidth, measured results agree with the simulation results. For the insertion loss, the measured results are approximately 0.3 dB increased compared with the simulation results.

Three types of design are presented and as a compatible design of low loss and wideband, a new modified V-shape patch element is proposed. It is confirmed by experiments that the improved transition exhibits an insertion loss of 0.6 dB from 76 to 77 GHz, and a bandwidth of 4.1 % (3.15 GHz) for the reflection coefficient below -15 dB.

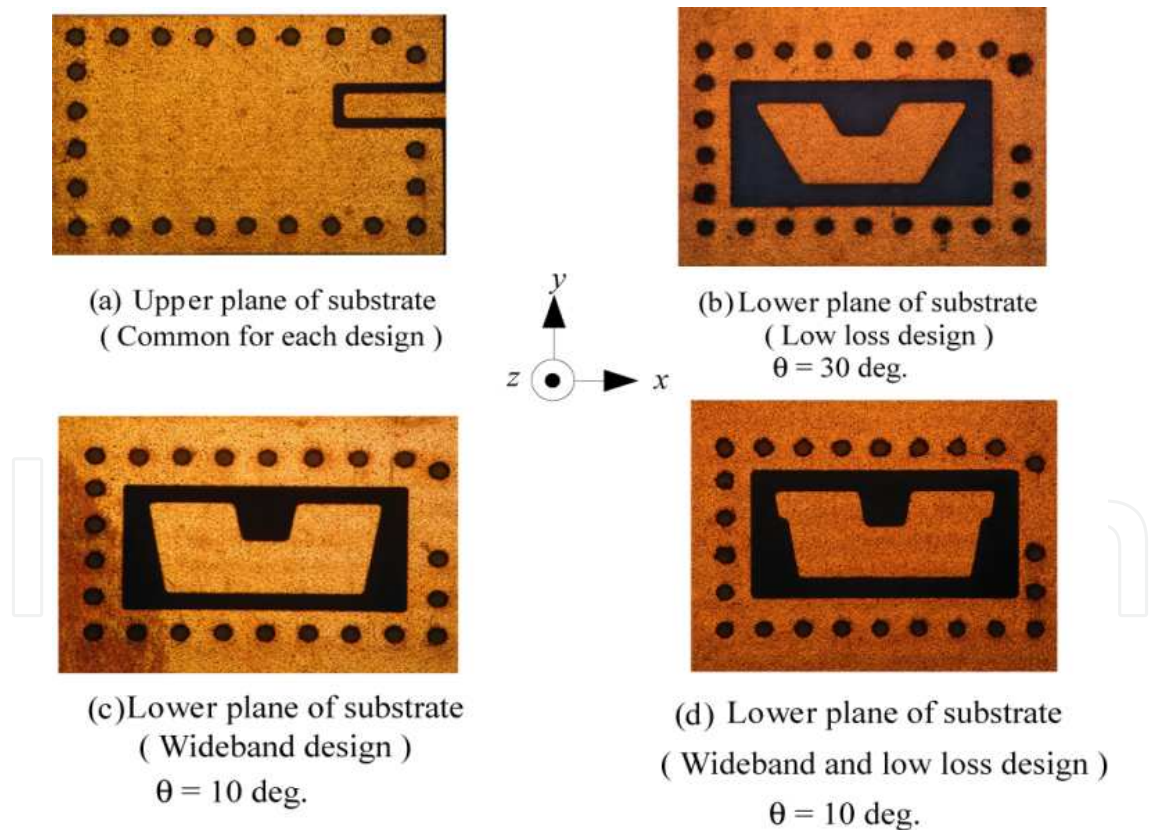


**Figure 33.** Fabricated transitons

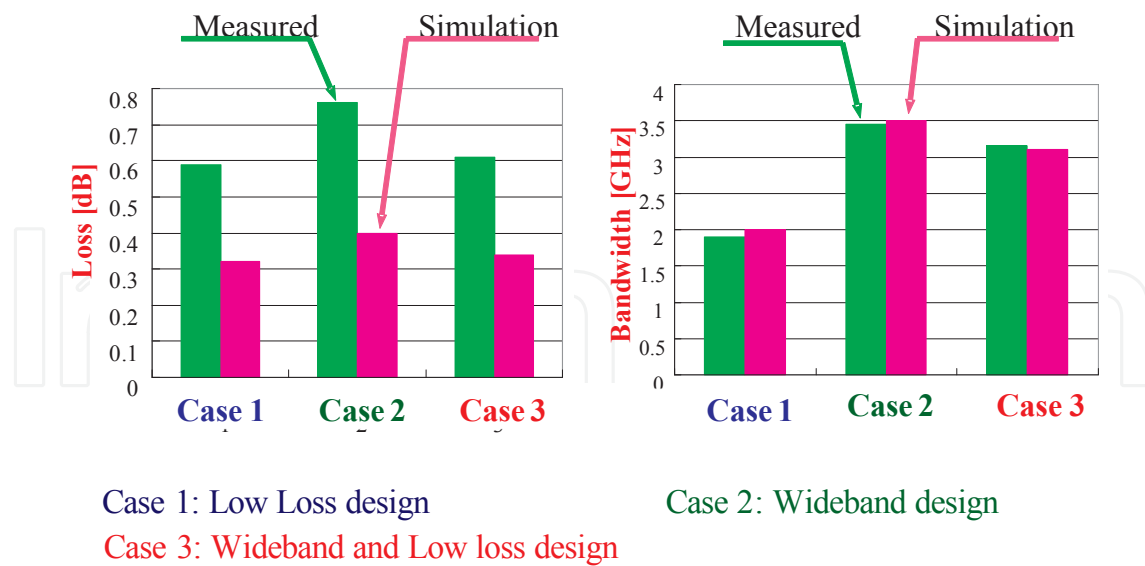


Figure 34. Comparison of each design

## Author details

Kazuyuki Seo

Address all correspondence to: kazuyuki.seo@pillar.co.jp; k\_seo1951@pure.ocn.ne.jp

Process Development Dept., Nippon Pillar Packing Co., Ltd. Sanda City, Japan

## References

- [1] Russel, M. E, Grain, A, Curran, A, Campbell, R. A, Drubin, C. A, & Miccioli, W. F. Millimeter-wave radar sensor for automotive intelligent cruise control(ICC)," IEEE Trans. Microw. Theory Tech., Dec. (1997). , 45(12), 2444-2453.
- [2] Russel, M. E, Drubin, C. A, Marinilli, A. S, & Woodington, W. G. Integrated automotive sensors, "IEEE Trans. Microw. Theory Tech., Mar. (2002). , 50(3), 674-677.
- [3] Yano, H. Y, Abdelmonem, A, Liang, J. F, & Zaki, K. A. Analysis and design of microstrip to waveguide transition, "IEEE Trans. Microw. Theory Tech., Dec. (1994). , 42(12), 2371-2379.
- [4] Kaneda, N, Qian, Y, & Itoh, T. A broadband microstrip-to-waveguide transition using quasi-Yagi antenna, "IEEE Trans. Microw. Theory Tech., Dec. (1999). MWSYM. 1999.780218, 47(12), 2562-2567.

- [5] Deslandes, D, & Wu, K. Integrated microstrip and rectangular waveguide in planar form, "IEEE Microw. Wireless Compon. Lett., Feb. (2001). , 11(2), 68-70.
- [6] Ho, T. Q, & Shih, Y. C. Spectral-domain analysis of E-Plane waveguide to microstrip transitions, "IEEE Trans. Microw. Theory Tech., Feb. (1989). , 37(2), 388-392.
- [7] Leong, Y, & Weinreb, S. Full band waveguide to microstrip probe transitions," IEEE MTT-S Int. Microw. Symp. Dig., Anaheim, CA, May (1999). MWSYM.1999.780219, 4, 1435-1438.
- [8] Grabherr, W, Hudder, B, & Menzel, W. Microstrip to waveguide transition compatible with mm-wave integrated circuits, "IEEE Trans. Microw. Theory Tech., Sep. (1994). , 42(9), 1842-1843.
- [9] Iizuka, H, Watanabe, T, Sato, K, & Nisikawa, K. Millimeter-wave microstrip line to waveguide transition fabricated on a single layer dielectric substrate," IEICE Trans. Commun., Jun. (2002). , E85-B(6), 1169-1177.
- [10] Iizuka, H, Sakakibara, K, & Kikuma, N. Millimeter-Wave Transition From Waveguide to Two Microstrip Lines Using Rectangular Patch Element," IEEE Trans. Microw. Theory Tech., May. (2007). TMTT.2007.895139, 55(5), 899-905.
- [11] Bahl, I. J, Trivedi, D. K, & , A. s Guide to Microstrip Line,"Microwaves, May (1977). , 174-182.
- [12] Strohm, K. M, Bloecher, H. L, Schneider, R, & Wenger, J. Development of Future Short Range Radar Technology," Radar Conference, 2005, EURAD 2005, European, Oct. (2005). , 165-168.
- [13] Seo, K, Sakakibara, K, & Kikuma, N. Microstrip-to-waveguide Transition using Waveguide with Large Broad-wall in Millimeter-wave Band," IEEE International Conference on Ultra-Wideband, ICUWB2010, Sep. (2010). ICUWB.2010.5614169, 1, 209-212.
- [14] Seo, K, Sakakibara, K, & Kikuma, N. Narrow-Wall-Connected Microstrip-to-Waveguide Transition Using V-Shaped Patch Element in Millimeter-Wave Band," IEICE Trans. Commun., Oct. (2010). , E93-B(10), 2523-2530.

